




# Magnetic ordering in strong anisotropic ferromagnetic bilayers with dipolar and antiferromagnetic interlayer exchange interactions: Monte Carlo approach

J. J. Melo Quintero , G. P. Saracco , and M. A. Bab \*

*Instituto de Investigaciones Físicoquímicas Teóricas y Aplicadas (INIFTA), UNLP, CCT La Plata-CONICET, sucursal 4, CC 16(1900) La Plata, Argentina*



(Received 17 January 2023; revised 1 December 2023; accepted 31 January 2024; published 27 February 2024)

In this work, multilayer films consisting of two strong-anisotropic ferromagnetic layers antiferromagnetically coupled by a nonmagnetic spacer are studied by Monte Carlo simulations. The system is modeled by an Ising-based Hamiltonian that depends on both the intralayer exchange and dipolar constants and on the interlayer exchange constant (IEC). The ground state of the monolayers (null IEC) corresponds to alternate stripe domains with width  $h$  defined by the ratio between the exchange and dipolar constants ( $\delta$ ). The results show that IEC alters the energy balance that controls the stripe domain formation, leading to a ground state characterized by in-plane stripes out-plane antiferromagnetically coupled. When temperature increases two regimes are identified: an IEC-dominated regime where the orientational and positional orders are simultaneously lost in both layers, driving the system to the tetragonal liquid (TL) phase, and a dipolar-dominated one where signs of layers decoupling and the onset of positional disorder are observed. The last could be related with an intermediate nematic phase (NM). From the study of the nonequilibrium dynamics, the phase transitions to TL phase are characterized as continuous and those to the NM one as Kosterlitz-Thouless type. Also, for both layers the critical temperatures are the same and increase with IEC magnitude. Furthermore, the obtained critical exponents depend on the IEC values, which is indicative of a weak universality. For the dipolar-dominated regime, the decoupling between layers is also evidenced by the difference between their critical exponents.

DOI: [10.1103/PhysRevE.109.024135](https://doi.org/10.1103/PhysRevE.109.024135)

## I. INTRODUCTION

The development and improvement of thin-film growth techniques have made it possible to obtain stacks of ultrathin magnetic films and nonmagnetic materials by controlling different growth conditions, as well as improving aspects related to epitaxial growth and stoichiometry in the samples [1–7]. The rich spectrum of the involved materials has triggered extensive studies to understand their fundamental nature as well as to design novel materials. In this way, magnetic multilayers have led to new phenomena that have extended their range of applications. The first among these is the existence of an interlayer exchange coupling (IEC) between magnetic layers by means of a nonmagnetic spacer. This coupling leads to systems with significantly different states and dynamic properties. In the case of metallic layers, the IEC is essentially of the Ruderman-Kittel-Kasuya-Yosida type and is associated with oscillations in the spin density of the nonmagnetic spacer caused by adjacent ferromagnets. The oscillations in turn lead to an IEC that also oscillates from ferromagnetic to antiferromagnetic with the distance between the ferromagnetic layers [1,8,9]. In this way, by changing the thickness of the nonmagnetic spacer it is possible to tune the interaction, whereas for thick spacers the IEC is suppressed. For insulating spacers, the IEC depends on the spin-polarized tunneling, and its strength decays exponentially with the spacer thickness [3]. Even though the metallic character of the ferromagnetic

layers was considered as an inherent element of the IEC, it was also reported in the case of multilayers based on ferromagnetic diluted semiconductors [6,10–14]. In these systems, the magnetic properties can be controlled not only by changing the spacer thickness but also by tuning the energy barrier of spacer and carrier density in the system. This fact has provided versatility for manipulating of magnetization reversal, consequently of resistance. Multilayers with antiferromagnetic IEC—referred to as synthetic antiferromagnets due to the overall structure—were crucial for the discovery of the phenomena of giant magnetoresistance and tunneling magnetoresistance that kick-started the fields of nanomagnetism and spintronics.

On the other hand, it is well known that in ferromagnetic thin films, the interplay between exchange interactions with perpendicular and shape anisotropies may lead to the emergence of stripe domains [15,16]. These configurations are characterized by an alternating (up-and-down) out-of-plane orientation of the magnetization. The presence of stripes has been reported when the perpendicular anisotropy-energy density,  $K_{\perp}$ , exceeds the magnetostatic one,  $1/2\mu_0 M_s^2$  ( $M_s$  is the saturation magnetization of the system), i.e., when the quality factor  $Q = (2K_{\perp})/(\mu_0 M_s^2) > 1$  [15,16]. This kind of stripe domain is characterized by thin domain walls, that is, very sharp transitions between stripes with opposite magnetization orientations. For moderate or low  $K_{\perp}$ , i.e., with  $Q < 1$ , it is possible to observe a re-orientation transition from planar to out-of-plane modulated magnetization states above a critical thickness that is characteristic of material [15,16]. These stripe domains present

\*mbab@inifta.unlp.edu.ar

wide domain walls, i.e., a smooth variation of the magnetization profile between stripes with opposite magnetization orientations.

In order to reveal the underlying mechanisms that define the thermal and magnetic behavior, common to magnetic thin films, several theoretical approaches—based on the Hamiltonians of Ising [17–27] and Heisenberg [28–34]—have been proposed. These models include anisotropy and dipolar terms. It is important to remark that the dipolar term has a long-range character and is related to the magnetostatic energy and, consequently, with the shape anisotropy. In this way, the competition between interactions acting on different scales leads to frustration of the ferromagnetic order, i.e., the short-range exchange interaction that favors an uniform ordered state is frustrated by a weaker long-range dipolar interaction.

For films with strong perpendicular anisotropy  $Q > 1$ , only spin-up and spin-down states need to be considered; thus, the anisotropy term can be approximated as constant, implying that it does not need to be considered for energy minimization. These systems have been intensively studied by means of the bidimensional Ising model with dipolar interactions. The phase diagram was obtained by Monte Carlo simulations and is characterized by phases with null total magnetization [17,18,23,24,27]. This includes at low temperatures the antiferromagnetic and stripe phases with width  $h = n$  (named  $h_n$ ), where  $n$  is an integer number measured in lattice units that increases with the ratio between the exchange ( $J$ ) and dipolar ( $g$ ) constants,  $\delta = J/g$ . At high temperatures, the positional order of the stripes vanishes, driving to a nematic (NM) or a tetragonal liquid (TL) phase depending on  $\delta$ . In the NM phase, the positional order is lost while the orientational one is conserved. On the other hand, the TL phase presents stripes of mutually perpendicular orientations forming labyrinthine patterns without both positional and orientational order.

If the temperature is raised enough, then a phase transition between the NM and TL phases takes place [20,23,24,27,35,36]. The order of the mentioned transitions has been the subject of a longstanding controversy [18,20,27]. Recently, the  $h_n$ -TL transitions were classified as continuous, and the critical exponents were estimated [22,23]. On the other hand,  $h_n$ -NM-TL transitions were conjectured to be of the Kosterlitz-Thouless type [24], in agreement with theoretical predictions [37].

Focusing on the multilayers formed by two strong-anisotropic ferromagnetic layers, the Ising model was used as a workbench due to its simplicity. The physical interest for many investigations comes from the IEC dependence on the order-disorder transition temperature. By considering that each layer may be thought of as an effective field acting on the other, a power-law dependence on the critical temperature with IEC strength was predicted with an exponent  $\frac{1}{\varphi}$ , where  $\varphi$  is named the shift exponent. For identical intralayer exchange constants, the shift exponent was predicted as  $\varphi = \gamma$ , where  $\gamma$  is the magnetic susceptibility critical exponent of the underlying bidimensional model [38–42]. However, for different exchange couplings the shift exponent prediction  $\varphi = \gamma/2$  [43] was not validated, and the reported values suggest that  $\varphi$  is not related to  $\gamma$  [39,44]. In order to determine the conditions for the compensation, i.e., the occurrence of zero total magne-

tization at nonzero magnetization of the layers, systems with nonequivalent layers were investigated. Diaz and Branco have used Monte Carlo simulations to investigate the compensation phenomenon determining that can be observed in systems constituted by three magnetic layers [26] or by multilayers with random diluted magnetic sites [45,46]. On the other hand, Mayberry *et al.* [47] used numerical simulations to extend the studies to multilayer systems with different thicknesses and number of layers, reporting temperature-magnetic field phase diagrams. In all cases, two phase transitions were observed. The first one occurs at low fields between a configuration where all layers are antiferromagnetically aligned and another intermediate that exhibits partial alignment with the field. The second transition is produced at higher values of the field and happens between the intermediate and paramagnetic phases. Moreover, the former transition has a first-order character, whereas the latter changes to continuous when the temperature is increased. Both transitions are connected through a tricritical point.

As mentioned, the dipolar interaction plays a key role in magnetic behavior because it defines the magnetostatic energy, although it has been neglected in all of the above-mentioned theoretical works about strong-anisotropic multilayers. This is in large part due to the difficulties introduced by its long-range character, which limits the system size used in the simulations and leads to strong finite-size effects. So, any convincing finite-size effect scaling, with a reliable determination of the phase behavior, becomes a difficult task to perform. In this context, studies of the dynamic evolution in the short-time regime—named short-time dynamics (STD)—is a powerful technique to study the phase transitions by means of Monte Carlo simulations. In fact, the STD method has been successfully applied to characterize the phase behavior in both equilibrium and nonequilibrium systems (see Ref. [48] and references therein), as well as to the case of a monolayer modeled by the Ising model with dipolar interactions [22–24].

The aim of this work is to study the phase behavior of multilayer systems formed by two strong-anisotropic ferromagnetic layers that exhibit stripe domains by using Monte Carlo simulations. The systems are modeled employing an Ising-like Hamiltonian with intralayer dipolar and ferromagnetic exchange interactions and interlayer antiferromagnetic coupling. For the sake of simulate different thicknesses of the nonmagnetic spacer, different interlayer constants are considered.

The paper is organized as follows: in Sec. II the utilized model is introduced, in Sec. III the simulation details and a summary of STD technique are outlined, in Sec. IV the results are presented and discussed. Finally, the conclusions are reported in Sec. V.

## II. FORMULATION OF THE MODEL

As mentioned in the previous section, for ultrathin films with strong perpendicular anisotropy, only spin-up and spin-down states need to be considered. This fact allows us to make use of the Ising model with dipolar interactions to simulate its behavior. The multilayer system studied is composed of two ferromagnetic monolayers coupled by an antiferromagnetic

IEC. Each layer is considered as a bidimensional Ising model on a square lattice, which is concentrically placed one over the other. The Hamiltonian of the model, hereinafter called antiferromagnetic-multilayer Ising dipolar, AF-MID, reads:

$$\begin{aligned} \mathcal{H} = & -J_1 \sum_{\langle i,j \rangle} S_i S_j - J_2 \sum_{\langle i,j \rangle} \sigma_i \sigma_j + g_1 \sum_{i,j} \frac{S_i S_j}{r_{i,j}^3} \\ & + g_2 \sum_{i,j} \frac{\sigma_i \sigma_j}{r_{i,j}^3} - J_3 \sum_i S_i \sigma_i, \end{aligned} \quad (1)$$

where  $S_i, \sigma_i (= \pm 1)$  are the spin variables of the layers labeled 1 and 2. The first two terms are the ferromagnetic intralayer interactions with exchange constants  $J_1 > 0$  and  $J_2 > 0$ , and the sum runs over all pairs of nearest-neighbor (NN) spins into each layer. The following two terms correspond to dipolar interactions with strengths  $g_1 > 0$  and  $g_2 > 0$ , and the sum runs over all pairs of spins  $(i, j)$  separated by a distance  $r_{ij}$  (measured in crystal units) within the same layer. The last term describes the coupling between layers with antiferromagnetic IEC  $J_3 < 0$ ; consequently, the sum involves NN spins located in different layers. On the other hand, the dipolar interactions between layer has not been taken into account, since IEC is mediated by a nonmagnetic spacer and its strength decays inversely proportional to the thickness. Furthermore, with the aim to investigate the thermal properties, the system is in contact with a thermal bath at the temperature  $T$ .

Based on the monolayer phase diagram of the Ising model with dipolar interaction [18,24] the following values were selected,  $J_2 = 2, J_1 = 1$ , and  $g_1 = g_2 = 1$ , for the exchange and dipolar constants measured in unit of  $J_1$ , respectively. These values refer to  $\delta_1 = 1$  and  $\delta_2 = 2$ , which match the monolayers with ground states  $h_1$  and  $h_2$ , respectively. The former presents a continuous transition to the TL phase, while the latter exhibits two Kosterlitz-Thouless- (KT) type transitions,  $h_2$ -NM and NM-TL, at temperatures higher than those corresponding to the monolayer with  $\delta = 1$  (see Ref. [24] and Table I). On the other hand, the IEC was chosen to take the following values,  $J_3 = -1.5, -1, 0$ , and  $J_3 = -0.5$ , also measured in units of  $J_1$ , which are related to the increasing thickness of the nonmagnetic spacer. The selected parameters allow us to study the effects of the perturbation introduced by the IEC on the magnetic and thermal behavior of the layers, which present not only different domain structures but also different critical behavior.

### III. SHORT-TIME DYNAMICS AND SIMULATION DETAILS

In the AF-MID model, the long-range character of the dipolar interactions, as well as the frustration introduced by the competition between interactions acting on different scales, makes the description of the phase transitions a difficult task to perform. In the case of the Monte Carlo simulations, the large simulation times required for equilibration limit the system sizes and hinder a finite-size scaling analysis. This fact can lead to misinterpretations of the results, for example, to confuse a weak first-order with a continuous phase transition. In this context, the STD method is a powerful tool to overcome those difficulties [48]. Concerning the monolayer version of the AF-MID that is equivalent to

the uncoupled layer,  $J_3 = 0$ , this method has already been successfully employed to determine the phase transition order, and when corresponds, to characterize the critical behavior [22–24].

The STD focuses on the time evolution of the order parameter and its moments within the early stages of the dynamics in a neighborhood of the phase transition point for different values of the control parameter. In this way, the simulations proceed under nonequilibrium conditions for a short time interval  $(t_{\text{mic}}, t_{\text{max}})$ , where  $t_{\text{mic}}$  and  $t_{\text{max}}$  are the times when the time correlation length  $\xi(t)$  is of the order of a lattice spacing and the system size  $L$ , respectively. As a consequence, STD is free of the critical slowdown because  $t_{\text{max}}$  is shorter than the equilibration time. In the present work, the control parameter is the temperature ( $T$ ). Since the system exhibits phases that are similar to those observed in the monolayer, the same observables can be employed to investigate the phase transitions, but in this case, they were measured for each layer. The order parameter is that introduced by Booth *et al.* [25]:

$$O_{hv} \equiv \frac{n_v - n_h}{n_v + n_h}, \quad (2)$$

where  $n_v$  ( $n_h$ ) is the number of vertical (horizontal) bonds of the NN antiparallel spins. With this definition,  $O_{hv} = +1$  ( $-1$ ) when the system is in the stripe horizontal (vertical) ordered phase and  $O_{hv} = 0$  in the TL or paramagnetic phases. Also, the susceptibility of the orientational order parameter  $\chi$ , the second-order Binder cumulant  $U$ , the autocorrelation function  $A$ , and the logarithmic derivative  $D$  with respect to the reduced temperature  $\zeta = (T - T_c)/T_c$  evaluated at the critical point  $T_c$  (if exists) are defined in the following way:

$$\chi = \frac{N}{T} (\langle O_{hv}^2 \rangle - \langle O_{hv} \rangle^2), \quad (3)$$

$$U = 1 - \frac{\langle O_{hv}^4 \rangle}{\langle O_{hv}^2 \rangle^2}, \quad (4)$$

$$A = \frac{1}{N} \left\langle \sum_i S_i(t) S_i(0) \right\rangle, \quad (5)$$

$$D = \left. \frac{\partial \log(\langle O_{hv} \rangle)}{\partial \zeta} \right|_{\zeta=0}, \quad (6)$$

where  $N = L^2$  is the number of spins of each layer and  $\langle \dots \rangle$  indicates the average over different thermal histories from equivalent initial conditions. To simplify the notation  $\langle O_{hv} \rangle$  and  $\langle O_{hv}^2 \rangle$  are changed to  $O_{hv}$  and  $O_{hv}^2$ , respectively.

For continuous transitions, at the critical point ( $T = T_c$ ), the time series of the observables exhibit a power-law behavior in the  $(t_{\text{mic}}, t_{\text{max}})$  interval when the system is initialized from the ground state (ordered configurations, OC) or the paramagnetic one (disordered configurations, DC) at  $T = 0$  or  $T = \infty$ , respectively [48,49]. The power-law exponents are related to the critical exponents defined at equilibrium. For  $T \simeq T_c$  the power laws are modified by scaling functions that depend on the reduced temperature  $\zeta$ , resulting in deviations from the proposed behavior at  $T = T_c$ . This allows us to determine the critical temperature as well as the critical exponents from the localization of the best power law (for more details see the review in Ref. [48] and references therein).

For the case of OC initial condition (ground state), the time evolution of the observables is as follows:

$$O_{hv}(t) \propto t^{-\frac{\beta}{\nu z}}, \quad (7)$$

$$\chi(t) \propto t^{\frac{\gamma}{\nu z}}, \quad (8)$$

$$U(t) \propto t^{\frac{d}{z}}, \quad (9)$$

$$D(t) \propto t^{\frac{1}{\nu z}}. \quad (10)$$

However, if the system starts from DC initial conditions (PM state) that correspond to  $O_{hv} = 0$ , then the power-law behavior of the  $O_{hv}^2(t)$  and  $A(t)$  is given by:

$$O_{hv}^2(t) = \frac{T}{N} \chi(t) \propto t^{\frac{\gamma}{\nu z}}, \quad (11)$$

$$A(t) \propto t^{-\lambda}, \quad (12)$$

where  $\beta$ ,  $\nu$ , and  $\gamma$  are the static critical exponents for  $O_{hv}$ ,  $\xi$ , and  $\chi$ , respectively;  $z$  and  $\lambda$  are the dynamic exponents of time correlation length  $\xi(t)$  and autocorrelation.

For the first-order phase transitions,  $\xi(t)$  also diverge as a power law but at the metastability limits of the coexisting phases. This fact leads to the identification of these points as the spinodals [48]. However, if the system is started from the OC condition, then the spinodal value of the order parameter,  $O_{hv}^{\text{sp}}$ , must be taken into account, so  $O_{hv}(t) - O_{hv}^{\text{sp}}$  decays as a power law. The difference between spinodal temperatures defines the strength of the transition and allows us to distinguish between continuous and weak first-order transitions [48].

Furthermore, the STD was also able to characterize topological KT transitions in models with short-range interactions, such as the XY, fully frustrated XY, and six-state clock models [50–54] and long-range ones [24]. For  $T \leq T_{\text{KT}}$  ( $T_{\text{KT}}$  is the transition temperature), the STD evolution of the order parameter and its moments follows a power law with exponent  $\mu$  that depends on  $T$  [48,52,54]. Therefore, the system is said to remain critical and the transition has an infinite order. It is important to note that in the monolayer version of the AF-MID model for  $\delta \geq 2$ , STD allowed us to determine that the  $h_n$ -NM and NM-TL phase transitions were both KT and to locate the transition temperatures  $T_{\text{KT}}$  [24].

In this work, Monte Carlo simulations were performed in square lattices with size  $L = 128$  using the Metropolis algorithm with heat bath dynamics. This size allows us to avoid artificial frustration and ensure that it is commensurate with the width of the stripes in the  $h_1$  and  $h_2$  phases. Periodic boundary conditions were implemented in the plane of the layers through the Ewald sums for proper treatment of the long-range character of the dipolar interactions, while free boundary conditions were set out in the perpendicular direction. In order to obtain the equilibrium configurations for each set of interaction constant values, the simulations were carried out until equilibration times of  $10^7$  Monte Carlo steps (MCS) for several temperatures. Furthermore, the STD observables were averaged over 5000 different realizations for each temperature.

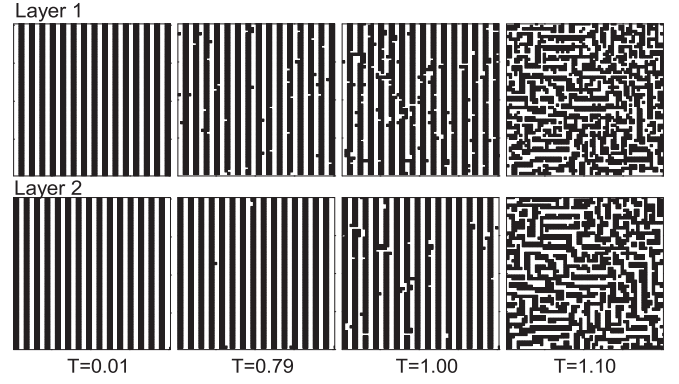


FIG. 1. Equilibrium spin configurations obtained after  $10^7$  MCS of layers 1 (upper row) and 2 (lower row) for different temperatures as indicated in the respective legends. The data correspond to  $J_3 = -1.5$ .

#### IV. RESULTS AND DISCUSSION

In this section equilibrium configurations obtained by simulations until  $10^7$  MCS, as well as the phase transitions between them, characterized by STD, are presented and discussed in decreasing order of IEC strength  $J_3$ . Furthermore, the results of the correlation functions are discussed in the last subsection.

##### A. Phase transitions for IEC $J_3 = -1.5$

Figure 1 shows snapshots of the AF-MID equilibrium spin configurations for IEC  $J_3 = -1.5$  at different temperatures. As can be observed, at low  $T$ , both layers show the in-plane  $h_2$  ordered configuration and are out-of-plane antiferromagnetically coupled. This configuration can be identified as the ground state of the system, hereafter named  $\text{AF}h_2$ . When the temperature increases, this phase remains stable up to  $T > 1.0$ , where the orientational order is lost and the TL phase emerges in both layers. However, they even exhibit a weak coupling. This result is indicative of a single  $\text{AF}h_2$ -TL phase transition.

Figures 2(a) and 2(b) exhibit the dynamic evolution of  $O_{hv}$  when the system is started from the OC, i.e.,  $\text{AF}h_2$ , at the temperatures indicated in the figures. The power-law fits for both layers were obtained from the data corresponding to the temperature  $T^{\text{OC}} = 1.082(2)$ . The error bars were determined as the neighboring temperatures where the evolution shows tiny deviations from the power law due to the scaling function.

On the other hand, Figs. 3(a) and 3(b) display the time evolution of  $O_{hv}^2$ , when the system is quenched from the DC, i.e., the paramagnetic phase. As in the OC case, the power-law regime is attained at the temperature  $T^{\text{DC}} = 1.082(2)$  and the error was estimated using the same procedure.

The fact that  $T^{\text{OC}}$  coincides with  $T^{\text{DC}}$  suggests a continuous phase transition between the  $\text{AF}h_2$  and TL phases. Thus,  $T = 1.082(2)$  can be interpreted as the critical temperature  $T_c$  of this transition. Furthermore, the exponents fitted for  $O_{hv}$  and  $O_{hv}^2$  can be identified as the STD dynamic exponents,  $\frac{\beta}{\nu z}$  and  $\frac{\gamma}{\nu z}$ , according to Eqs. (7) and (11), respectively. They are listed in Table I. This assumption is supported by the behavior

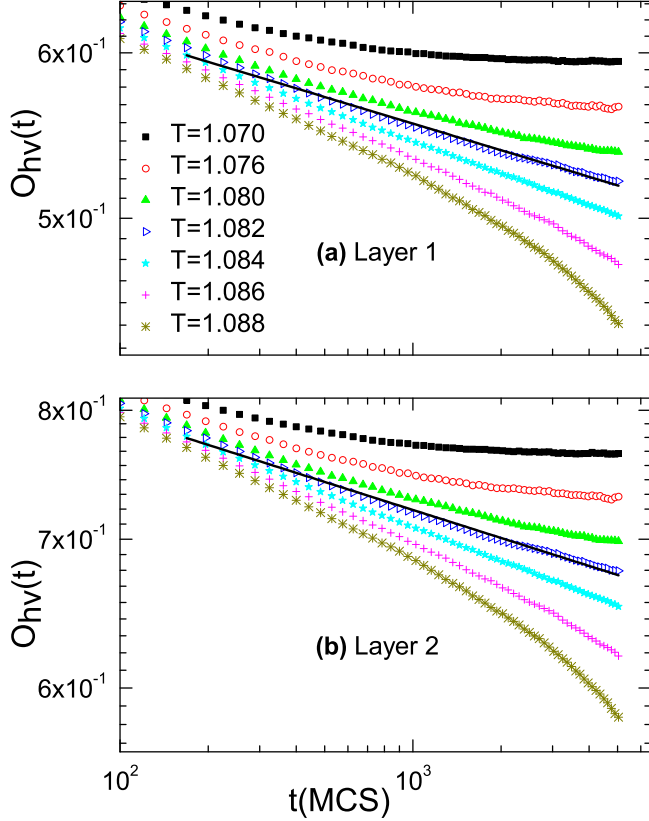


FIG. 2. Dynamic evolution of  $O_{hv}(t)$  for layers 1 (a) and 2 (b) at the temperatures stated in the legend, when the system was initialized from OC. The power-law fits are indicated by solid lines and correspond to  $T^{\text{OC}} = 1.082$  for both layers, while deviations from this behavior are clearly observed, allowing us to define the error bars.

of the susceptibility measured from the OC also at  $T_c = 1.082$ , which is displayed in Figs. 4(a) and 4(b) for layers 1 and 2, respectively. In fact, the data can be well fitted by Eq. (8) and the exponents present a difference smaller than 3% with respect to the values obtained from the  $O_{hv}^2$  evolution. The estimated  $T_c$  is higher than that reported for the transition  $h_1$ -TL of the monolayer with  $\delta = 1$  [22] and for NM-TL exhibited by the monolayer with  $\delta = 2$  [24] (see Table I and Fig. 5) that are associated with  $J_1$  and  $J_2$ , respectively. Therefore, an IEC whose strength is the average of the intralayer ferromagnetic exchange constants stabilizes the stripe phase, allowing the presence of the orientational order at higher  $T$ . Furthermore, this IEC value may suppress the intermediate NM phase between the  $h_2$  and TL phases in layer 2. Moreover, the transition  $\text{AF}h_2$ -TL is performed by a simultaneous loss of the orientational and positional order in direct way without a NM intermediate phase.

Figure 6 exhibits the dynamic evolution from the initial OC at  $T_c = 1.082$  of the Binder cumulant,  $U(t)$ , and logarithmic derivative of the orientational order parameter evaluated at the critical point,  $D(t)$ . The data were fitted with Eqs. (9) and (10), for  $U(t)$  and  $D(t)$ , respectively. The obtained exponents are also included in Table I.

By combining the STD exponents corresponding to the initial OC ( $\text{AF}h_2$ ) with  $d = 2$ , the dynamic and static crit-

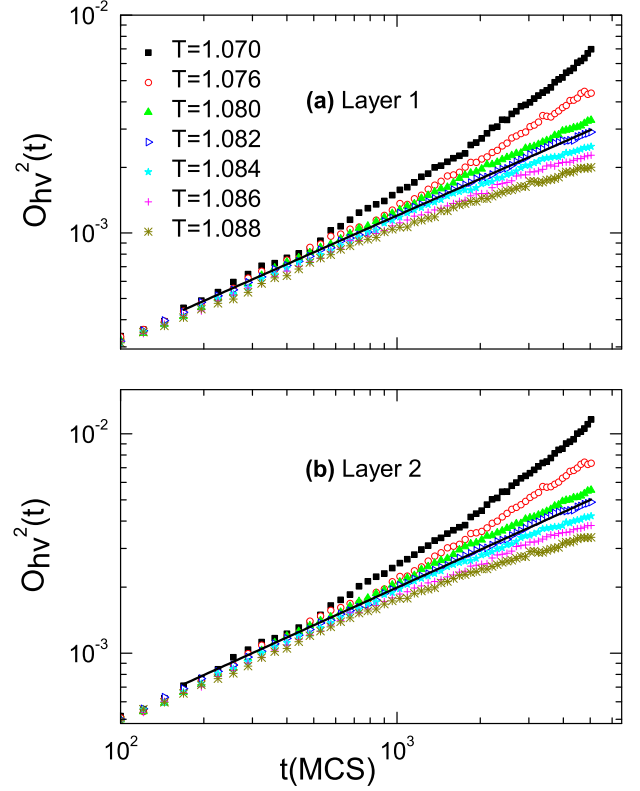


FIG. 3. Time evolution of  $O_{hv}^2$  for layers 1 (a) and 2 (b) at the stated temperatures when the system was initialized from DC. The power-law fits are indicated by solid lines and correspond to the temperature  $T^{\text{DC}} = 1.082$  for both layers. In addition, the closest temperatures allow us to determine the error bars.

ical exponents  $z$ ,  $\nu$ ,  $\gamma$ , and  $\beta$  can be calculated for each layer. These values are displayed in Table II, together with those calculated for the monolayer with  $\delta = 1$ . As shown in Table II, the critical exponents  $\gamma$  and  $\nu$  are the same within error bars for both layers. On the other hand, the values of the exponents  $z$  and  $\beta$  obtained for each layer differ by about 5% and 7%, respectively. This result is indicative that similar critical behavior occurs in both layers. By focusing the attention on layer 1, its critical exponents significantly differ from those calculated for the monolayer with  $\delta = 1$ . This reflects that the IEC with layer 2 leads not only to stabilize the orientational order with an  $h_2$  phase at higher temperatures but also to alter its critical behavior.

### B. Phase transitions for IEC $J_3 = -1.0$

By using the previously described procedure, the equilibrium spin configurations at different temperatures were obtained. The results show the  $\text{AF}h_2$  phase at low temperatures and the TL one at  $T \geq 1.0$ . On the other hand, a similar STD behavior of the observables was obtained (not shown for the sake of space). Indeed, the dynamic relaxation of  $O_{hv}$  from the  $\text{AF}h_2$  phase (OC) exhibits a power law at  $T^{\text{OC}} = 1.012(4)$  for both layers. In turn,  $O_{hv}^2$  presents the best power law at  $T^{\text{DC}} = 1.008(4)$ , when the system is quenched from DC. These temperatures are the same within error bars, which is a hallmark of the continuous phase transition at

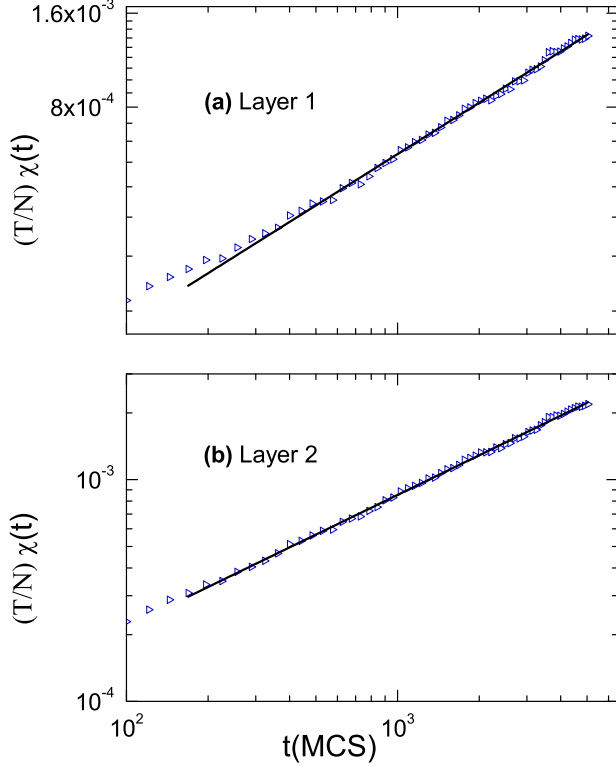


FIG. 4. Log-log plots of the susceptibility  $\chi(t)$  at the critical point  $T_c = 1.082$ , when the system was initialized from OC ( $AFh_2$ ) for (a) layer 1 and (b) layer 2. The solid lines correspond to the fit of data with Eq. (8).

$T_c = 1.012(4)$ . Furthermore, the estimated  $T_c$  is again larger than the transition temperatures to TL fase of both  $\delta = 1$  and  $\delta = 2$  monolayer cases but smaller than that of  $J_3 = -1.5$  case (see Table I and Fig. 5). This means that a IEC of magnitude  $J_3 = -1.0$  still favors the presence of the orientational order at larger temperatures. As will be discussed in Sec. IV D this transition could be related with a NM-TL.

In order to calculate the critical exponents, Table I reports the estimated values of the STD exponents. For layer 2, the values of the exponent  $\frac{\gamma}{\nu z}$  obtained from both initial conditions (OC and DC) are very close. On the other hand, for layer 1,

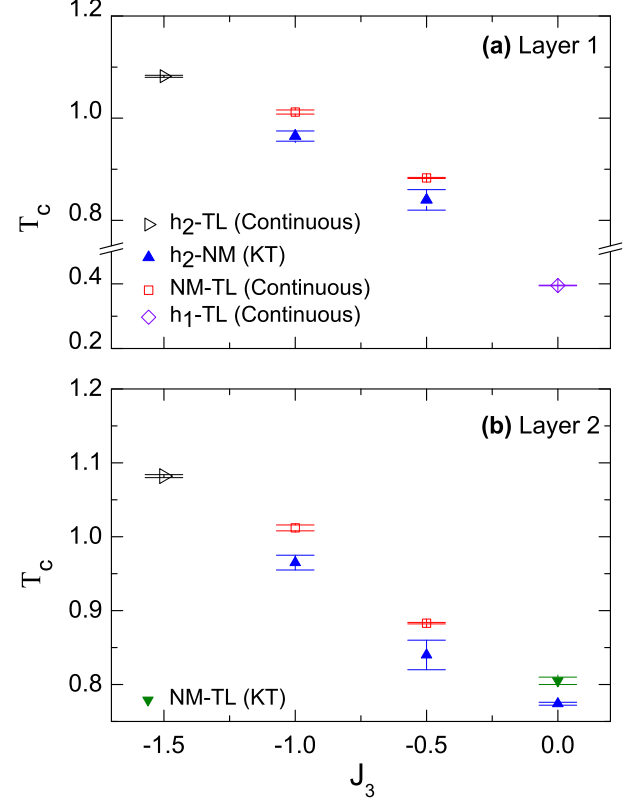


FIG. 5. Critical temperatures obtained by using the STD analysis from  $AFh_2$  initial configuration for (a) layer 1 and (b) layer 2. The corresponding phase transitions are indicated in the legend. The figure also shows the monolayers data with  $\delta = 1$  and  $\delta = 2$ , taken from Refs. [22,24].

the difference between these exponents is about of 5%. This result supports the continuous character of the transition to TL phase.

Table II presents the calculated critical exponents from STD. As can be observed, the exponents  $\gamma$  and  $\nu$  are the same within the error bars, while  $z$  and  $\beta$  present departures larger than  $J_3 = -1.5$  case. This result suggests a similar critical behavior for both layers. Moreover, all estimated critical exponents are smaller than those calculated for  $J_3 = -1.5$ . In

TABLE I. Critical temperatures and STD exponents for the investigated values of  $J_3$ . For the sake of comparison, the critical temperatures and STD exponents of the monolayer model with  $\delta = 1.0$  are also reported [22]. In addition, the KT temperatures of both  $h_2$ -NM and NM-TL phase transitions are exhibited for the monolayer case corresponding to  $\delta = 2.0$  [24]. More details are presented in the text.

$J_3$	Layer	$T_c$		$\frac{\beta}{\nu z}$	$\frac{\gamma}{\nu z}$		$\frac{1}{\nu z}$	$\frac{d}{z}$
		OC	DC		OC	DC		
-1.5	1	1.082(2)	1.082(2)	0.0423(4)	0.546(5)	0.561(4)	0.457(3)	0.626(5)
	2	1.082(2)	1.082(2)	0.0419(4)	0.594(4)	0.571(4)	0.501(4)	0.671(5)
-1.0	1	1.012(4)	1.008(4)	0.0447(2)	0.598(7)	0.643(7)	0.590(6)	0.691(6)
	2	1.012(4)	1.008(4)	0.0442(2)	0.682(4)	0.669(7)	0.653(5)	0.770(5)
-0.5	1	0.883(1)	0.882(2)	0.0212(2)	0.235(6)	0.31(4)	0.49(1)	0.277(6)
	2	0.883(1)	0.880(2)	0.0212(2)	0.586(4)	0.671(5)	0.577(6)	0.639(5)
Monolayer $\delta = 1.0$		0.395(1)	0.396(2)	0.0804(5)	0.740(8)	0.747(5)	0.552(6)	0.903(8)
Monolayer $\delta = 2.0$		0.774(2) and 0.805(5)		-	-	-	-	-

TABLE II. Critical exponents calculated from STD exponents of the transition to TL phase, obtained from initial OC for each layer. The corresponding results of the monolayer system with  $\delta = 1$  are also displayed [22].

$J_3$	Layer	$z$	$\nu$	$\gamma$	$\beta$
-1.5	1	3.19(3)	0.685(7)	1.19(2)	0.093(1)
	2	2.98(2)	0.670(8)	1.19(2)	0.084(1)
-1.0	1	2.89(3)	0.586(8)	1.01(2)	0.076(1)
	2	2.60(2)	0.590(6)	1.04(1)	0.068(1)
-0.5	1	7.2(2)	0.283(8)	0.48(2)	0.043(1)
	2	3.13(2)	0.554(7)	1.02(1)	0.037(1)
Monolayer $\delta = 1.0$		2.21(2)	0.82(1)	1.34(2)	0.146(2)

this way, the results are indicative of a weak universality in the AF-MID model.

### C. Phase transitions for IEC $J = -0.5$

The equilibrium spin configurations at different temperatures are exposed in Fig. 7. As in the previous cases, the system exhibits the  $AFh_2$  phase at low temperatures, but at larger values of  $T$  some differences in the behaviors of the layers appear. In fact, at  $T \sim 0.80$ , layer 2 begins to lose the positional order but the orientational one is conserved, indicating a transition to a possible NM phase. On the other hand, layer 1 begins to exhibit positional disorder at  $T \sim 0.5$  (not shown). Even if exists an evident orientational order at  $T \sim 0.80$ , the presence of a NM phase cannot be assured. By increasing the temperature even more, the orientational order is also lost, and at  $T = 0.9$ , the existence of a TL phase is clear in both layers.

The dynamic evolution of  $O_{hv}(t)$  from the OC, is quite similar to the former investigated cases. In fact, Figs. 8(a) and 8(b) show that the best power-law behavior was determined to be at

$T^{\text{OC}} = 0.883(1)$  for both layers. The error bars were assessed by following the previously described procedure. Figures 9(a) and 9(b) show the time evolution of  $O_{hv}^2(t)$ , when the system is quenched from the DC initial condition. A critical regime is observed and the best power-law behavior was obtained at  $T^{\text{DC}} = 0.882(2)$  for layer 1 and at  $T^{\text{DC}} = 0.880(2)$  for layer 2. These temperatures match within error bars with that obtained for  $O_{hv}(t)$ . As a consequence, this result is indicative of a continuous phase transition to the TL phase. Also, this transition temperature is lower than those of the previous  $J_3$  cases but remains higher than that corresponding to NM-TL transition displayed by the monolayer with  $\delta = 2$ .

However, at lower temperatures,  $O_{hv}^2$  does not show the characteristic deviations due to the scaling function that were already observed for the previous cases. Instead, Fig. 10 shows that this observable displays a power-law behavior in the interval  $0.55 \leq T \leq 0.84$ , with exponents that increase with  $T$ , as shown in Fig. 11. As mentioned in Sec. III, this dynamic behavior is considered a signature of a KT phase transition since the system remains critical for all temperatures below the transition temperature  $T_{\text{KT}}$  [24,48]. The

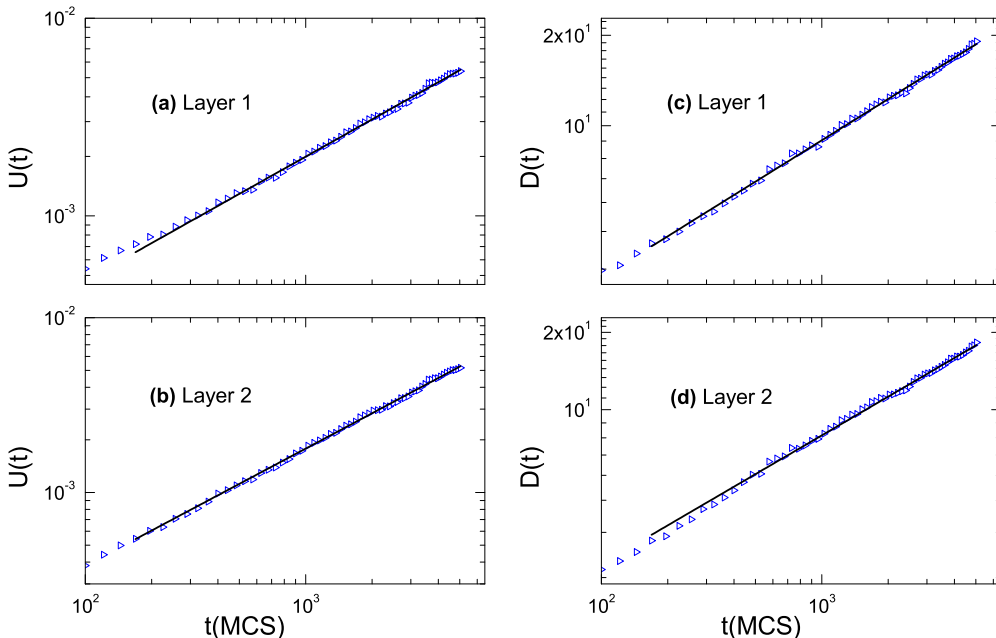


FIG. 6. Log-log plots of the time series of  $U(t)$  and  $D(t)$  at the critical point,  $T_c = 1.082$ , of  $J_3 = -1.5$  from OC. [(a) and (c)] Layer 1 and [(b) and (d)] layer 2. The solid lines indicated the fits of data with Eqs. (9) and (10).

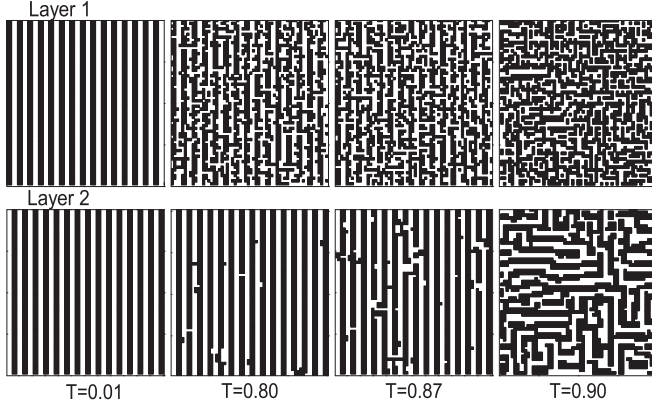


FIG. 7. Equilibrium spin configurations obtained after  $10^7$  MCS of layers 1 (upper row) and 2 (lower row) at different temperatures, as indicated in the respective legends. The data correspond to  $J_3 = -0.5$ .

snapshot of layer 2—exhibited in Fig. 7—shows at  $T = 0.87$  the orientational order characteristic of NM phase, so the KT transition would occur between this phase and the ordered  $AFh_2$ . In the following section, the study of the spatial correlation and autocorrelation functions will allow us to identify the intermediate phase as an NM one. The exposed results in Figs. 10 and 11 suggest that the transition  $AFh_2$ -NM is of the KT type with a transition temperature  $T_{KT} \simeq 0.84$ , because

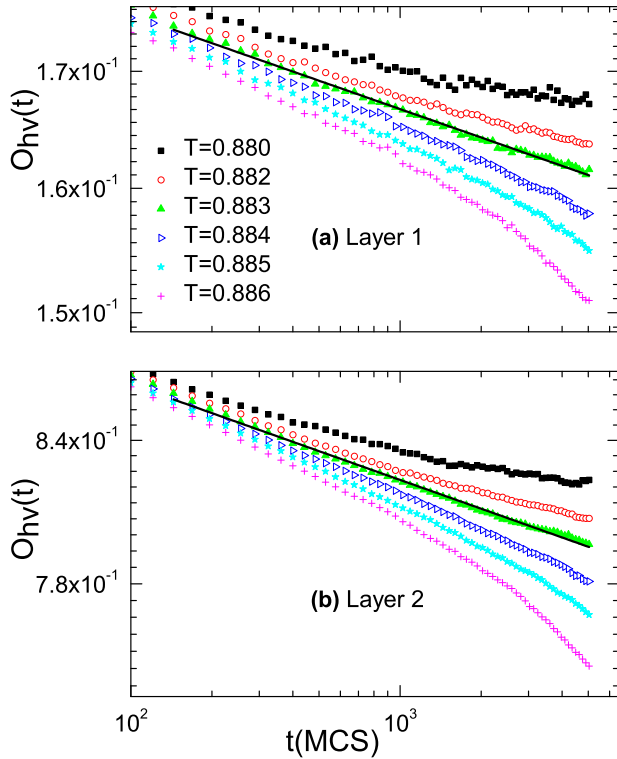


FIG. 8. Dynamic evolution of  $O_{hv}(t)$  at the temperatures indicated in the legend, when the system was initialized from OC. (a) Layer 1 and (b) layer 2. The best power-law fits with Eq. (7), indicated with solid lines, were found for  $T^{OC} = 0.883$  in both layers, while deviations from this behavior can clearly be observed.

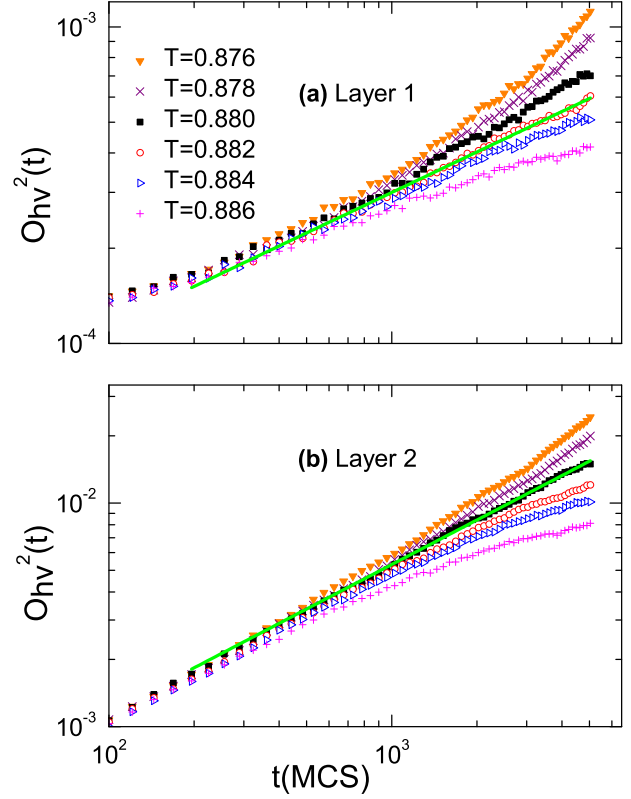


FIG. 9. Time evolution of  $O_{hv}^2(t)$  at the indicated temperatures when the system was initialized from DC. (a) Layer 1 and (b) layer 2. The best fits with Eq. (11), indicated with solid lines, correspond to the temperatures  $T^{DC} = 0.882$  and  $T^{DC} = 0.880$  for layers 1 and 2, respectively.

it is the last temperature where the power-law behavior of  $O_{hv}^2$  is observed. It is important to note that a similar dynamic behavior was already observed in the monolayer system with  $\delta = 2$ . However, in that case, both phase transitions ( $h_2$ -NM and NM-TL) were reported are KT type [24]. Here the value of the IEC may be responsible for changing the character of the transition NM-TL, i.e., from KT to continuous for layer 2.

Regarding layer 1, the lack of positional order prevents to be conclusive about the presence of an NM phase in the neighborhood of KT transition (see upper row of Fig. 7). This may be due to the IEC low value, which is not large enough to keep the positional order in the  $h_2$  phase with the increase of the thermal fluctuations, like in the former IEC values. Nevertheless, a noticeable orientational order can still be detected without a clear antiferromagnetic-coupled configuration between layers. So the IEC should be meant as a weak external magnetic field applied to layer 1, whose direction is regulated by the NM phase in layer 2. This field competes with thermal fluctuations, leading to small ordering. Finally, layer 1 presents a TL phase that mixes spin domains of widths  $h = 1$  and  $h = 2$  without any sign of AF coupling. In the next section, this subject will be discussed based on the study of the spatial correlation functions.

Furthermore, if the theoretical values of  $\nu = 0.5$  and  $\eta = 0.25$  for KT transition are used in the hyperscaling relationship  $\frac{z}{\nu} = (d - \eta)$ , then the dynamic exponent  $z$  can be



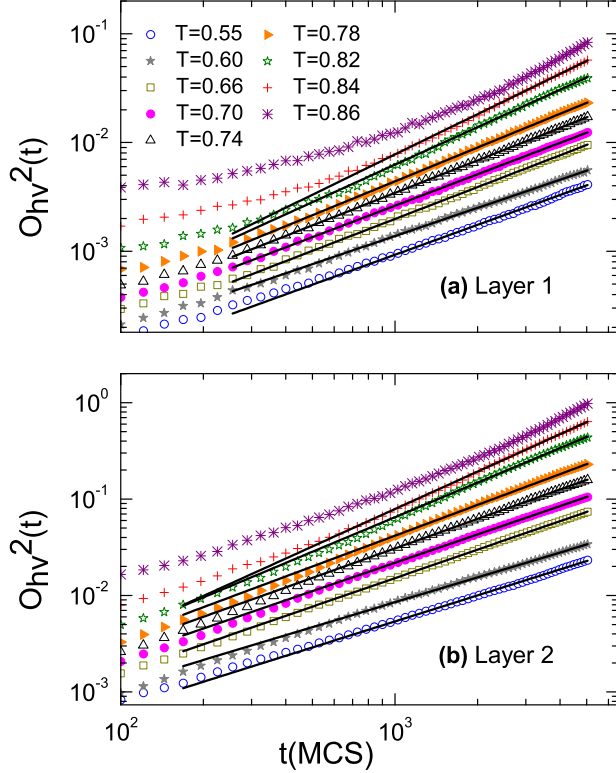


FIG. 10. Log-log plot of the  $O_{hv}^2$  time evolution for (a) layers 1 and (b) layer 2 at the indicated temperature, when the system was initialized from DC. The data were multiplied by the same factor for the sake of clarity. The fits with power laws are indicated with solid lines. More details in the text.

estimated for the AF $h_2$ -NM transition since  $\mu = \frac{\gamma}{\nu z}$  for  $T = 0.84$  (see Fig. 11). The obtained values are  $z = 1.42(1)$  and  $z = 1.357(5)$  for layers 1 and 2, respectively. These are close to the estimated for the  $h_2$ -NM transition in the monolayer with  $\delta = 2$ , i.e.,  $z = 1.57(2)$  [24].

Coming back to the critical behavior of the transition to TL phase, Table I reports the critical temperatures and the STD exponents obtained from the fit of time series of  $O_{hv}(t)$ ,  $\chi(t)$ ,  $U(t)$ , and  $D(t)$  at  $T^{\text{OC}} = 0.883$  and  $O_{hv}^2(t)$  at  $T^{\text{DC}} = 0.882$ . As can be observed, there is a noticeable difference between the values of  $\frac{\gamma}{\nu z}$  obtained by the fits of  $O_{hv}^2(t)$  and  $\chi(t)$  from the DC and OC initial conditions, respectively. This discrepancy may be related to the proximity of the KT transition that interferes the continuous transition by affecting the correlations developing from each initial condition. Table II summarizes the critical exponents calculated from the STD exponents. For layer 2, the static exponents  $\beta$  and  $\nu$  follow a decreasing trend with  $J_3$ , while  $\gamma$  remains closer to the value corresponding to  $J_3 = -1.0$ . Besides, the dynamic exponent  $z$  remains near 3, which is close to the  $h_2$ -TL values reported for the monolayer system in the with  $1.23 \leq \delta \leq 1.9$  range [23]. On the other hand, the exponents of layer 1 are significantly different from those of layer 2. The estimated value of the  $z$  exponent indicates a strong slowing down in the dynamics of layer 1. As mentioned,  $J_3 = -0.5$  is insufficient to ensure the positional order in layer 1 and the antiferromagnetic coupling between layers at

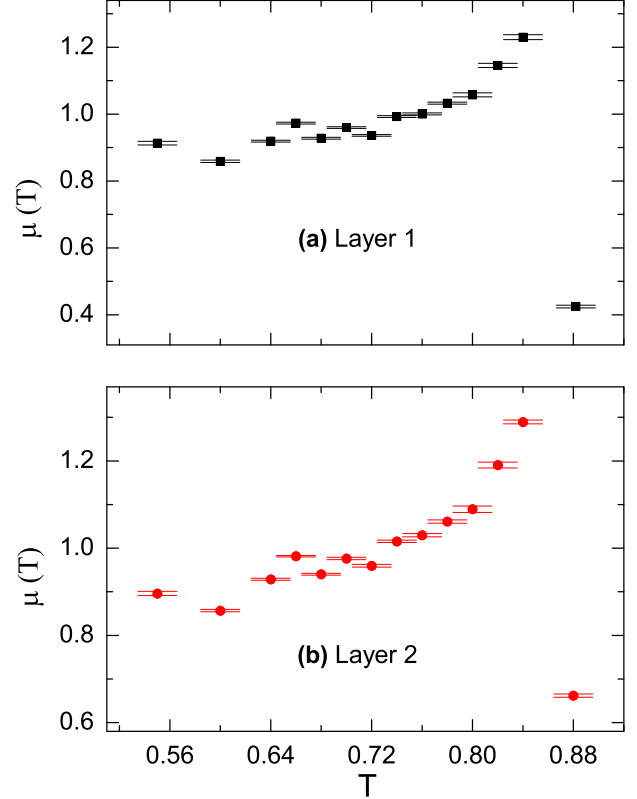


FIG. 11. STD exponents of  $O_{hv}^2$  for layers (a) 1 and (b) 2 in the interval  $0.55 \leq T \leq 0.84$ . The STD exponents of the continuous phase transition to TL phase are also shown.

temperatures  $T > 0.882$ . Moreover, the monolayer with the same parameters is already in the TL phase at temperatures where the positional disorder begins to be observed in the AF-MID. So the slowing down in the dynamics could be consequence of the competition between the weak local field generated by layer 2 and thermal fluctuations.

#### D. Correlations

In this section, the results related to the spatial correlation and time autocorrelation functions are exhibited and discussed. Since the system presents ordered anisotropic phases, it is mandatory to study the longitudinal and transversal correlation functions, i.e., parallel and perpendicular to the spin stripes, respectively. These functions are defined as:

$$C_x(r) = \frac{1}{N} \left\langle \sum_y \sum_x s(x+r, y) s(x, y) \right\rangle, \quad (13)$$

$$C_y(r) = \frac{1}{N} \left\langle \sum_x \sum_y s(x, y+r) s(x, y) \right\rangle, \quad (14)$$

where the subscripts  $y$  and  $x$  are designated as the longitudinal and transversal directions,  $s$  is the spin variable on each layer [ $\sigma$  or  $S$ , see Eq. (1)], and  $r$  is the distance between the spins at positions  $(x+r, y)$  or  $(x, y+r)$  and  $(x, y)$ . It is important to remark that the measurements of Eqs. (13) were performed once the system reached equilibrium states. The angle brackets indicate realization averages.

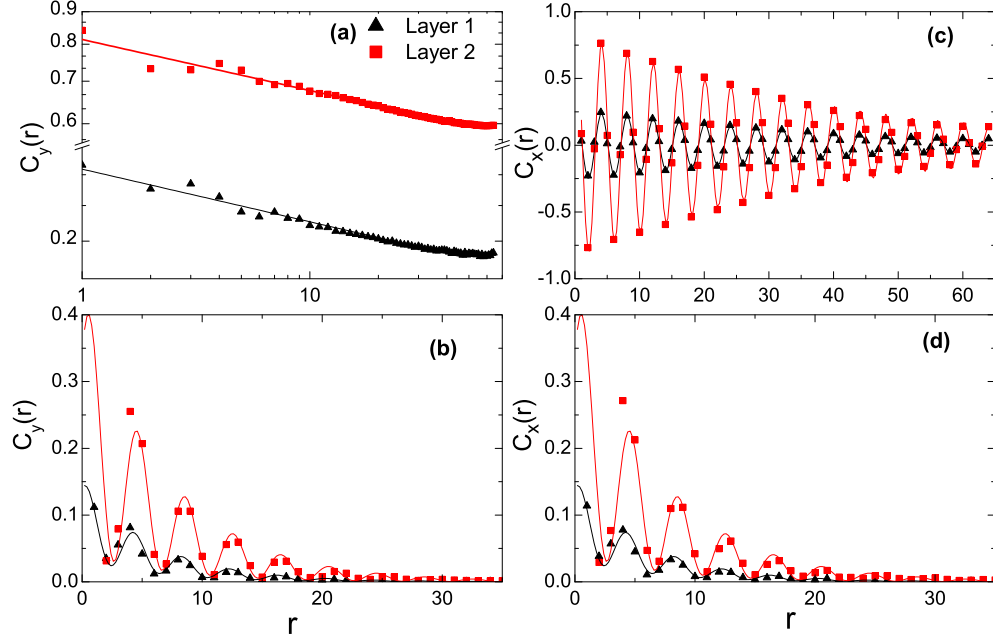


FIG. 12. Spatial correlation functions  $C_y(r)$  and  $C_x(r)$  corresponding to  $J_3 = -0.5$ , and temperatures [(a) and (c)]  $T = 0.87$  and [(b) and (d)]  $T = 0.90$ . The fits of the data with functions  $f_x(r)$ ,  $f_y(r)$ , and  $g(r)$  (defined in the text) are indicated with solid lines.

Figure 12 presents the behavior of the correlation functions at two temperatures,  $T = 0.87$  [Figs. 12(a) and 12(c)] and  $T = 0.90$  [Figs. 12(b) and 12(d)], for IEC  $J_3 = -0.5$ .

Figure 12(a) shows the transversal correlations  $C_y(r)$ , which can be fitted with oscillating functions modulated with exponential decays, i.e.,  $f_y(r) = A_0 e^{-r/\xi} \sin[k(r + \phi)]$ , where  $A_0$  is the amplitude,  $\xi$  is the spatial correlation length,  $\phi$  is the phase shift, and  $k = \frac{\pi}{2}$  since the stripe width is  $h = 2$ . The estimated parameters are  $\xi = 39(2)$  [ $\xi = 37(2)$ ] lattice units  $A_0 = 0.27(1)$  [ $A_0 = 0.86(3)$ ] and  $\phi = -0.89(1)$  [ $\phi = -0.86(3)$ ] for layer 1 (layer 2). Figure 12(c) presents  $C_x(r)$  data that are well fitted with power law  $f_x(r) \sim r^{-\omega}$ , with exponent  $\omega = 0.080(2)$  [ $\omega = 0.093(2)$ ] for layer 1 (layer 2).

The fact that longitudinal correlations decay algebraically while transversal correlations do it exponentially suggests that the orientational order is preserved, but positional ordering is lost. These features allow us to classify the intermediate phase between  $AFh_2$  and TL as NM, according to the theoretical approach by Abanov *et al.* [55] and observed in the Monte Carlo simulations performed in Refs. [19,24] for the monolayer with  $\delta = 2$ . Regarding the difference between the amplitudes ( $A_0$ ) estimated for both layers, it may reasonably be linked to the major positional disorder exhibited by layer 1.

Figures 12(b) and 12(d) display the correlation functions at  $T = 0.90$ , i.e., in the TL phase (see the last column of snapshots in Fig. 7). The difference between the magnitudes between layers is also evident, but  $C_x(r) \sim C_y(r)$  of each layer, unlike the NM phase. This finding is an indication of the isotropic character of the TL phase. In view of this result a single expression is proposed that contains both the lack of orientational order and the oscillations characteristic of this phase. So the proposed correlation function is  $g(r) = e^{-x/\xi} [A_0 + A_1 \sin(k(r - A_2))]$  for both directions, where again  $k = \frac{\pi}{2}$  and  $A_i$  are fitting constants. As can be observed, the data can be well fitted with the last function. The estimated

correlation length ranged in the interval  $5.5 \leq \xi \leq 6.7$  lattice units, which is much smaller than in the transversal correlation lengths of the NM phase.

The short-time behavior of the autocorrelation function  $A(t)$ , defined in Eq. (12), is displayed in Fig. 13. This function exhibits, for both layers, a power-law behavior up to  $T = 0.84$ , like  $O_{hv}^2$  in Fig. 10. Furthermore, the estimated exponent  $\lambda$  also increases with  $T$ , as shown in the inset. The fact that both  $A(t)$  and  $O_{hv}^2(t)$  behave similarly up to the same temperature suggests that the system remains critical (see Ref. [48]), supporting the conjecture about a Kosterlitz-Thouless transition between the  $AFh_2$ -NM phases. It is important to mention that the same analysis was performed on the systems with the other  $J_3$  IEC values, but similar behaviors on the correlations (spatial and autocorrelation) were found only for  $J_3 = -1.0$ . So the NM intermediate phase seems to emerge after a KT transition at low values of the interlayer coupling. In this way, Abanov *et al.* have predicted that the stripe orientational order could support topological excitations, as bound dislocation pairs with opposite Burger vectors, which proliferate when the temperature increase until  $T_{KT}$ . From this temperature, unbound dislocations multiply, producing the lack of positional order. The authors also guess that the NM phase is stable over a finite range of temperatures until orientational order disappears and the disordered TL structure emerges. So the bound and unbound dislocation pairs would play a similar role to the well-known bound and unbound vortices in the XY models.

## V. CONCLUSIONS

Synthetic antiferromagnets in thin-film geometries are the object of intensive research with the aim of better understanding their magnetic and thermal properties. The description of these systems should take into account that they are composed of ferromagnetic multilayers, with an antiferromagnetic IEC

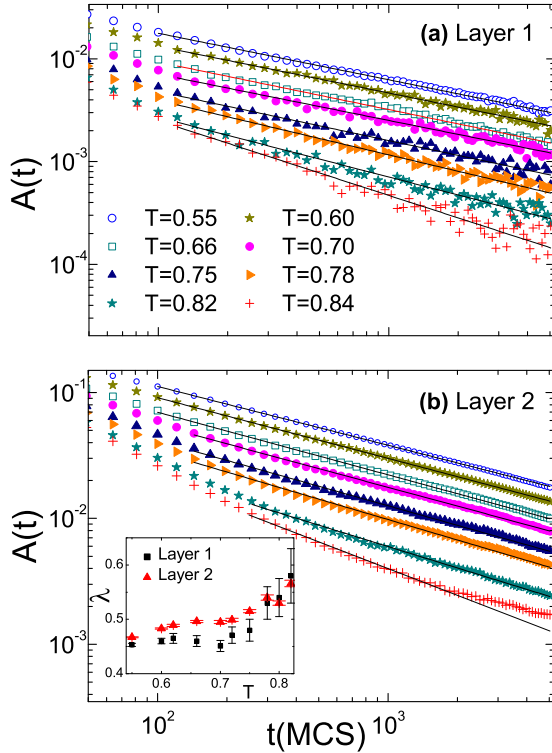


FIG. 13. Log-log plots of the autocorrelation function versus time of (a) layer 1 and (b) layer 2 corresponding to  $J_3 = -0.5$  for the temperatures indicated in the legend. The solid lines indicate the fits of the data with Eq. (12). The inset shows the exponent  $\lambda$  as a function of the temperature.

provided by the spacer layer. The strength of IEC can be controlled by the thickness of the spacer. In particular, multilayers that exhibit a strong perpendicular anisotropy have been modeled by layered Ising spins with antiferromagnetic IEC. However, when the multilayer also displays stripe domains, the dipolar interaction plays a fundamental role in the energy balance, so it must be included in the Hamiltonian.

In the present work, multilayer systems formed by two strong-anisotropic ferromagnetic layers that exhibit stripe domains at low temperatures, separated by a nonmagnetic spacer, were studied using Monte Carlo simulations. The systems were modeled by an Ising-like Hamiltonian with dipolar and ferromagnetic exchange intralayer interactions and antiferromagnetic IEC (AF-MID). For the ferromagnetic layers, identified by 1 and 2, the exchange and dipolar constants were selected as  $J_2 = 2$  and  $g_1 = g_2 = 1$  relative to  $J_1$  that correspond to  $\delta_1 = 1$  and  $\delta_2 = 2$ , respectively. In the case of the monolayers, these parameters match the ground states  $h_1$  and  $h_2$  that are characterized by stripe domain widths  $h = 1$

and  $h = 2$ , respectively. For the sake of simulating different thicknesses of the nonmagnetic spacer, different IEC constants were considered ( $J_3 = -0, 5, -1.0$ , and  $-1.5$ ).

The results show that IEC alters the energy balance that controls the stripe domain formation. Due to this, the obtained ground state was the in-plane  $h_2$  phase and out-of-plane antiferromagnetic coupled one ( $AFh_2$ ), minimizing the interlayer energy for all studied IEC. In this way, two competing reversal modes are developed under thermal fluctuations. One of them, the IEC-dominated regime ( $J_3 = -1.5$ ), where  $AFh_2$  phase losses simultaneously both orientational and positional order by a continuous phase transition to TL. The other one, the dipolar-dominated regime ( $J_3 \leq -1.0$ ), where the first  $AFh_2$  loses the positional order, leading to an intermediate NM phase through a KT-type transition, and subsequently the orientational order is missing via a continuous phase transition to the TL phase. As consequence, the last regime presents the same phase transitions that the monolayer with  $\delta = 2$ , but exhibiting a continuous character for the NM-TL transition. On the other hand, this IEC value is insufficient to keep the positional order in layer 1 above the critical temperature  $h_1$ -TL of the monolayer with  $\delta = 1$ . However, a detailed study of the spin correlation functions confirm the presence of an NM phase.

Concerning the critical behavior, the same critical temperature is found for all the layers. The obtained values increase with the absolute value of  $J_3$  and remain larger than those corresponding to the monolayers with  $\delta = 1$  or  $\delta = 2$ . Consequently, the thermal stability of the ordered phase enhances with  $|J_3|$ , in agreement with previous results of the short-range models. On the other hand, the set of critical exponents of the continuous phase transitions differ from both estimated for the monolayer and for the three different values of  $J_3$ . This last result indicates a weak universality. Furthermore, for  $J_3 = -0.5$  the layer decoupling is also evident by the significant difference between the critical exponents obtained for each layer.

As a final thought, the AF-MID model could be useful for modeling systems whose properties can be controlled well via advanced thin-film deposition techniques. Also, it can be applied as a tool for tailoring the different energy terms studying the effects of the competition between interactions.

## ACKNOWLEDGMENTS

This work was supported by Projects PIP0511 of CONICET and X11/784 of UNLP, Argentina. We also thank UnCaFiQT-INIFTA (SNCAD) for computational resources.

- [1] R. A. Duine, K. J. Lee, Stuart S. P. Parkin, and M. D. Stiles, Synthetic antiferromagnetic spintronics, *Nat. Phys.* **14**, 217 (2018).  
 [2] M. A. Herman and H. Sitter, *Molecular Beam Epitaxy: Fundamentals and Current Status*, Vol. 7 (Springer Science & Business Media, New York, 1996).

- [3] B. Chen, H. Xu, C. Ma, S. Mattauch, D. Lan, F. Jin, Z. Guo, S. Wan, P. Chen, G. Gao, F. Chen, Y. Su, and W. Wu, All-oxide based synthetic antiferromagnets exhibiting layer-resolved magnetization reversal, *Science* **357**, 191 (2017).

- [4] J. Leiner, H. Lee, T. Yoo, S. Lee, B. J. Kirby, K. Tivakornsasithorn, X. Liu, J. K. Furdyna, and M. Dobrowolska, Observation of antiferromagnetic interlayer exchange coupling in a  $\text{Ga}_{1-x}\text{Mn}_x\text{As}/\text{GaAs}:\text{Be}/\text{Ga}_{1-x}\text{Mn}_x\text{As}$  trilayer structure, *Phys. Rev. B* **82**, 195205 (2010).
- [5] G. Chern, L. Horng, W. K. Shieh, and T. C. Wu, Antiparallel state, compensation point, and magnetic phase diagram of  $\text{Fe}_3\text{O}_4/\text{Mn}_3\text{O}_4$  superlattices, *Phys. Rev. B* **63**, 094421 (2001).
- [6] P. Sankowski and P. Kacman, Interlayer exchange coupling in (Ga, Mn)As-based superlattices, *Phys. Rev. B* **71**, 201303(R) (2005).
- [7] S. El Khiraoui, M. Sajjeddine, M. Hehn, S. Robert, O. Lenoble, C. Bellouard, M. Sahlaoui, and K. Benkirane, Magnetic studies of Fe/Cu multilayers, *Phys. B: Condens. Matter* **403**, 2509 (2008).
- [8] J. P. Renard, Magnetic multilayers, *J. Mater. Sci. Technol.* **9**, 1 (1993).
- [9] H. J. Waring, Y. Li, C. Moutafis, I. J. Vera-Marun, and T. Thomson, Magnetization dynamics in synthetic ferromagnetic thin films, *Phys. Rev. B* **104**, 014419 (2021).
- [10] T. A. Samburskaya, A. Yu. Sipatov, V. V. Volobuev, P. Dziawa, W. Knoff, L. Kowalczyk, M. Szot, and T. Story, Magnetization studies of antiferromagnetic interlayer coupling in EuS-SrS semiconductor multilayers, *Acta Phys. Pol. A* **124**, 133 (2013).
- [11] H. Kepa, J. Kutner-Pielaszek, J. Blinowski, A. Twardowski, C. F. Majkrzak, T. Story, P. Kacman, R. R. Galazka, K. Ha, H. J. M. Swagten, W. J. M. de Jonge, A. Yu. Sipatov, V. Volobuev, and T. M. Giebultowicz, Antiferromagnetic interlayer coupling in ferromagnetic semiconductor EuS/PbS(001) superlattices, *Europhys. Lett.* **56**, 54 (2001).
- [12] Y. S. Chung, J. H. and Song, T. Yoo, S. J. Chung, S. Lee, B. J. Kirby, X. Liu, and J. K. Furdyna, Investigation of weak interlayer exchange coupling in GaMnAs/GaAs superlattices with insulating nonmagnetic spacers, *J. Appl. Phys.* **110**, 013912 (2011).
- [13] S. Lee, S. Chung, H. Lee, X. Liu, M. Dobrowolska, and J. K. Furdyna, Interlayer exchange coupling in (Ga, Mn)As ferromagnetic semiconductor multilayer systems, *J. Semicond.* **40**, 081503 (2019).
- [14] C. J. P. Smits, A. T. Filip, H. J. M. Swagten, B. Koopmans, W. J. M. de Jonge, M. Chernyshova, L. Kowalczyk, K. Graszka, A. Szczerbakow, T. Story, W. Palosz, and A. Y. Sipatov, Antiferromagnetic interlayer exchange coupling in all-semiconducting EuS/PbS/EuS trilayers, *Phys. Rev. B* **69**, 224410 (2004).
- [15] E. Sallica Leva, R. C. Valente, F. Martínez Tabares, M. Vásquez Mansilla, S. Roshdestwensky, and A. Butera, Magnetic domain crossover in FePt thin films, *Phys. Rev. B* **82**, 144410 (2010).
- [16] N. R. Álvarez, J. E. Gómez, M. Vásquez Mansilla, B. Pianciola, D. G. Actis, G. J. Gilardi, L. Leiva, J. Milano, and A. Butera, Magnetic coupling of stripe domains in FePt/Ni80Fe20 bilayers, *J. Phys. D: Appl. Phys.* **50**, 115001 (2017).
- [17] E. Rastelli, S. Regina, and A. Tassi, Phase diagram of a square Ising model with exchange and dipole interactions: Monte Carlo simulations, *Phys. Rev. B* **76**, 054438 (2007).
- [18] S. A. Pighín and S. A. Cannas, Phase diagram of an Ising model for ultrathin magnetic films: Comparing mean field and Monte Carlo predictions, *Phys. Rev. B* **75**, 224433 (2007).
- [19] S. A. Cannas, M. F. Michelon, D. A. Stariolo, and F. A. Tamarit, Ising nematic phase in ultrathin magnetic films: A Monte Carlo study, *Phys. Rev. B* **73**, 184425 (2006).
- [20] S. A. Cannas, M. F. Michelon, D. A. Stariolo, and F. A. Tamarit, Interplay between coarsening and nucleation in an Ising model with dipolar interactions, *Phys. Rev. E* **78**, 051602 (2008).
- [21] H. Komatsu, Y. Nonomura, and M. Nishino, Temperature-field phase diagram of the two-dimensional dipolar Ising ferromagnet, *Phys. Rev. E* **98**, 062126 (2018).
- [22] C. M. Horowitz, M. A. Bab, M. Mazzini, M. L. Rubio Puzzo, and G. P. Saracco, Phase transitions and critical phenomena in the two-dimensional Ising model with dipole interactions: A short-time dynamics study, *Phys. Rev. E* **92**, 042127 (2015).
- [23] M. A. Bab, C. M. Horowitz, M. L. Rubio Puzzo, and G. P. Saracco, Phase transitions and multicritical behavior in the Ising model with dipolar interactions, *Phys. Rev. E* **94**, 042104 (2016).
- [24] M. A. Bab and G. P. Saracco, Evidence of Kosterlitz-Thouless phase transitions in the Ising model with dipolar interactions, *Phys. Rev. E* **100**, 022143 (2019).
- [25] I. Booth, A. B. MacIsaac, J. P. Whitehead, and K. De'Bell, Domain structures in ultrathin magnetic films, *Phys. Rev. Lett.* **75**, 950 (1995).
- [26] I. J. L. Diaz and N. S. Branco, Compensation temperature in spin-1/2 Ising trilayers: A Monte Carlo study, *Physica A* **540**, 123014 (2020).
- [27] J. S. M. Fonseca, L. G. Rizzi, and N. A. Alves, Stripe-tetragonal phase transition in the two-dimensional Ising model with dipole interactions: Partition function zeros approach, *Phys. Rev. E* **86**, 011103 (2012).
- [28] M. Stier and W. Nolting, Carrier-mediated interlayer exchange, ground-state phase diagrams, and transition temperatures of magnetic thin films, *Phys. Rev. B* **84**, 094417 (2011).
- [29] H. Komatsu, Y. Nonomura, and M. Nishino, Anisotropy-temperature phase diagram for the two-dimensional dipolar Heisenberg model with and without magnetic field, *Phys. Rev. B* **100**, 094407 (2019).
- [30] H. Komatsu, Y. Nonomura, and M. Nishino, Phase diagram of the dipolar Ising ferromagnet on a kagome lattice, *Phys. Rev. B* **106**, 014402 (2022).
- [31] A. Razouk, M. Sahlaoui, and M. Sajjeddine, Dependence of the magnetization on the interface morphology in ultra-thin magnetic/non-magnetic films: Monte Carlo approach, *Appl. Surf. Sci.* **255**, 8695 (2009).
- [32] M. Carubelli, O. V. Billoni, S. A. Pighín, S. A. Cannas, D. A. Stariolo, and F. A. Tamarit, Spin reorientation transition and phase diagram of ultrathin ferromagnetic films, *Phys. Rev. B* **77**, 134417 (2008).
- [33] S. Djedai, E. Talbot, and P. E. Berche, A Monte Carlo study of the magnetization reversal in  $\text{DyFe}_2/\text{YFe}_2$  exchange-coupled superlattices, *J. Magn. Magn. Mater.* **368**, 29 (2014).
- [34] E. Restrepo-Parra, J. Londoño-Navarro, and J. Restrepo, Interface exchange parameters in  $\text{La}_{2/3}\text{Ca}_{1/3}\text{Mn}_3\text{O}/\text{La}_{1/3}\text{Ca}_{2/3}\text{Mn}_3\text{O}$  bilayers: A Monte Carlo approach, *J. Magn. Magn. Mater.* **344**, 1 (2013).
- [35] L. G. Rizzi and N. A. Alves, Phase transitions and auto-correlation times in two-dimensional Ising model with dipole interactions, *Phys. B: Condens. Matter* **405**, 1571 (2010).

- [36] L. G. Rizzi and N. A. Alves, Multicanonical simulation and trapping due to high free-energy barriers in an Ising model for ultrathin magnetic films, *J. Comput. Interdiscip. Sci.* **2**, 79 (2011).
- [37] A. Mendoza-Coto, D. A. Stariolo, and L. Nicolao, Nature of long-range order in stripe-forming systems with long-range repulsive interactions, *Phys. Rev. Lett.* **114**, 116101 (2015).
- [38] M. Suzuki, Scaling with a parameter in spin systems near the critical point. I\*, *Prog. Theor. Phys.* **46**, 1054 (1971).
- [39] A. Lipowski, Critical temperature in the two-layered Ising model, *Physica A* **250**, 373 (1998).
- [40] J. M. J. van Leeuwen, Singularities in the critical surface and universality for Ising-like spin systems, *Phys. Rev. Lett.* **34**, 1056 (1975).
- [41] Z. B. Li, Z. Shuai, Q. Wang, H. J. Luo, and L. Schülke, Critical exponents of the two-layer Ising model, *J. Phys. A: Math. Gen.* **34**, 6069 (2001).
- [42] J. C. Moodie, M. Kainth, M. R. Robson, and M. W. Long, Transition temperature scaling in weakly coupled two-dimensional Ising models, *Physica A* **541**, 123276 (2020).
- [43] J. Oitmaa and I. G. Enting, Critical behaviour of a two-layer Ising system, *J. Phys. A: Math. Gen.* **8**, 1097 (1975).
- [44] A. V. Myshlyavtsev, M. D. Myshlyavtseva, and S. S. Akimenko, Classical lattice models with single-node interactions on hierarchical lattices: The two-layer Ising model, *Physica A* **558**, 124919 (2020).
- [45] I. J. L. Diaz and N. S. Branco, Monte Carlo study of an anisotropic Ising multilayer with antiferromagnetic interlayer couplings, *Physica A* **490**, 904 (2018).
- [46] I. J. L. Diaz and N. S. Branco, Monte Carlo simulations of an Ising bilayer with non-equivalent planes, *Physica A* **468**, 158 (2017).
- [47] J. Mayberry, K. Tauscher, and M. Pleimling, Equilibrium and nonequilibrium properties of synthetic metamagnetic films: A Monte Carlo study, *Phys. Rev. B* **90**, 014438 (2014).
- [48] E. V. Albano, M. A. Bab, G. Baglietto, R. A. Borzi, T. S. Grigera, E. S. Loscar, D. E. Rodríguez, M. L. Rubio Puzo, and G. P. Saracco, Study of phase transitions from short-time nonequilibrium behaviour, *Rep. Prog. Phys.* **74**, 026501 (2011).
- [49] Y. Ozeki and N. Ito, Nonequilibrium relaxation method, *J. Phys. A: Math. Theor.* **40**, R149 (2007).
- [50] K. Okano, L. Schülke, K. Yamagishi, and B. Zheng, Monte carlo simulation of the short-time behaviour of the dynamic XY-model, *J. Phys. A: Math. Gen.* **30**, 4527 (1997).
- [51] Y. Echinaka and Y. Ozeki, Improved dynamical scaling analysis using the kernel method for nonequilibrium relaxation, *Phys. Rev. E* **94**, 043312 (2016).
- [52] Y. Ozeki, K. Ogawa, and N. Ito, Nonequilibrium relaxation analysis of Kosterlitz-Thouless phase transition, *Phys. Rev. E* **67**, 026702 (2003).
- [53] H. J. Luo, L. Schülke, and B. Zheng, Dynamic approach to the fully frustrated XY model, *Phys. Rev. Lett.* **81**, 180 (1998).
- [54] P. Czermer and U. Ritschel, Universal short-time dynamics in the Kosterlitz-Thouless phase, *Phys. Rev. E* **53**, 3333 (1996).
- [55] A. Abanov, V. Kalatsky, V. L. Pokrovsky, and W. M. Saslow, Phase diagram of ultrathin ferromagnetic films with perpendicular anisotropy, *Phys. Rev. B* **51**, 1023 (1995).